Biol. Cell (2016) **108,** 307–323 DOI: 10.1111/boc.201600024

Review

Volume scanning electron microscopy for imaging biological ultrastructure

Benjamin Titze[1] **and Christel Genoud**

Friedrich Miescher Institute for Biomedical Research, Basel, Switzerland

Electron microscopy (EM) has been a key imaging method to investigate biological ultrastructure for over six decades. In recent years, novel volume EM techniques have significantly advanced nanometre-scale imaging of cells and tissues in three dimensions. Previously, this had depended on the slow and error-prone manual tasks of cutting and handling large numbers of sections, and imaging them one-by-one with transmission EM. Now, automated volume imaging methods mostly based on scanning EM (SEM) allow faster and more reliable acquisition of serial images through tissue volumes and achieve higher *z*-resolution. Various software tools have been developed to manipulate the acquired image stacks and facilitate quantitative analysis. Here, we introduce three volume SEM methods: serial block-face electron microscopy (SBEM), focused ion beam SEM (FIB-SEM) and automated tape-collecting ultramicrotome SEM (ATUM-SEM). We discuss and compare their capabilities, provide an overview of the full volume SEM workflow for obtaining 3D datasets and showcase different applications for biological research.

Introduction

Researchers have continually strived to invent or improve imaging methods to obtain more faithful representations of biological specimens. In the past dozen years, the development of volume electron microscopy techniques has been transformative. With their capability to capture thousands of serial EM images with minimal human intervention, these techniques have made it easier, faster and more reliable to acquire tissue volumes for ultrastructural analysis. Extending EM imaging to the third dimension offers new possibilities for investigating complex biological structures ranging from organelles to neuronal networks. Here, three-dimensional (3D) information is often indispensable to gain a full understanding of function.

[1]To whom correspondence should be addressed (email: benjamin.titze@fmi.ch)

Key words: Brain/nervous system, Cellular imaging, Electron microscopy, Systems biology.

Abbreviations: ATUM, automated tape-collecting ultramicrotome; EM, electron microscopy; FIB, focused ion beam; FOV, field of view; rOTO, reduced osmium tetroxide – thiocarbohydrazide – osmium tetroxide; SBEM, serial block-face electron microscopy; SBF-SEM, serial block-face scanning electron microscopy; SEM, scanning EM; ssSEM, serial section scanning electron microscopy; ssTEM, serial section TEM; TEM, transmission EM.

In the following, we will retrace the beginnings of volume EM and the development of automated approaches in recent years. We will then discuss three volume scanning EM techniques in detail and describe the full workflow from sample preparation to 3D image analysis. Finally, we will showcase several volume SEM applications in cell and tissue biology and offer a glimpse into what the future may hold for these techniques.

Early (volume) EM for biological imaging

EM (Knoll and Ruska, 1932; Ardenne, 1938) became a powerful method for biological imaging soon after its invention in the 1930s. With resolutions ranging from nanometres down to below an ångström (Nellist et al., 2004), EM has been used to investigate macromolecules and the organisation of cell structures at the organelle level (Knott and Genoud, 2013). The resolution offered by EM exceeds – typically by orders of magnitude – that of both diffraction-limited and more recent 'super-resolution' light microscopy (Huang et al., 2009). However, while a light microscope's use of photons allows imaging depths of hundreds of microns (Helmchen and Denk, 2005) or

even several millimetres (Chung et al., 2013), the EM beam electrons can penetrate only thin surface layers. Electron penetration depths range from a few nanometres to several microns, depending on beam energy (Kanaya and Okayama, 1972). Using EM to image a volume, for example an entire cell, therefore requires a slicing approach that divides the sample – ideally without any loss – into manageable sections.

Manual sectioning followed by imaging of individual sections with transmission EM (serial section TEM, ssTEM) appeared in the 1950s (Birch-Andersen, 1955; Bang and Bang, 1957) and has since been a widely used technique to image tissue volumes. With a typical thickness of between 50 and 100 nm, sections are cut with a diamond knife and manually transferred onto a supporting film or grid for TEM imaging (Harris et al., 2006). The acquired images are manually aligned to obtain a 3D representation of the tissue. Notable among research efforts that pushed the limits of this technique was the reconstruction of the entire nervous system of the roundworm *Caenorhabditis elegans* (White et al., 1986).

Electron tomography (for an introduction, see McIntosh et al., 2005; Frank, 2006) is a different approach to obtain 3D structural information by using electrons (see Marsh et al., 2004, for a biological application). Here, the interior of a single section (thickness may range from 50 nm to >1 μm) is computationally reconstructed from a tilt series of TEM images. The grid holding the specimen is rotated in small increments, and an image is acquired for each angle of rotation. Electron tomography can be combined with ssTEM, which reduces the number of sections required to reconstruct a given tissue volume (Soto et al., 1994). However, many images are needed for each tilt series, and the long beam exposure causes tissue distortion and shrinkage (Briggman and Denk, 2006).

A significant drawback to imaging serial ultrathin sections with TEM is manual cutting and handling of sections. This is slow and error-prone, and requires extreme manual dexterity. Sections can easily be damaged or lost during collection, staining or handling of grids. Section loss or severe damage in a series breaks the continuity of structures in the imaged volume. Artefacts may be introduced during sectioning, and thin sections may fold or become distorted during handling, making alignment difficult.

A revival driven by automation, digitalisation and better SEMs

To overcome the disadvantages of manual serial sectioning for TEM, Leighton (1981) suggested to combine a scanning electron microscope with a miniature ultramicrotome installed in the vacuum chamber of the scanning electron microscope. He built a prototype (US Patent No. 4377958, 'Remotely operated microtome') and remarked: 'The value of the technique will be greatest when full automation is completed, and large numbers of images are processed by computer.'

This was realised in 2004 with the appearance of serial block-face scanning electron microscopy (SBF-SEM, Denk and Horstmann, 2004), later renamed serial block-face electron microscopy (SBEM). In a SBEM system, a diamond knife iteratively removes a thin surface layer of the sample. After each cut, the exposed smooth block-face is imaged. This *in situ* method for acquiring tissue volumes was a significant advance for biological imaging: It was the first demonstration of fully automated volume EM using a slicing approach. Other serial EM studies followed, also pursuing high levels of automation and reliability.

In situ milling with high-energy ions combined with SEM imaging, a technique called focused ion beam SEM (FIB-SEM), was shown to deliver excellent results for biological specimens (Heymann et al., 2006; Knott et al., 2008). Here, instead of a diamond knife, a focused beam of gallium ions removes thin layers of material from the sample block-face.

The automatic tape-collecting lathe ultramicrotome (Hayworth et al., 2006) was another milestone for volume SEM. The latest version is called automated tape-collecting ultramicrotome SEM (ATUM-SEM) (Schalek et al., 2012). The ATUM automatically collects serial thin sections on tape after they are cut off a sample block with a diamond knife. The tape holding the sections is then manually transferred onto wafers for SEM imaging.

A similar approach that combines manual serial sectioning with SEM imaging was introduced as Array Tomography (Micheva and Smith, 2007; reviewed in Wacker and Schroeder, 2013). Here, thin sections (50–200 nm) are manually collected in ordered arrays on glass slides. They can be imaged with both light microscopy and EM in a complementary fashion with various fluorescent labelling options. Related

techniques are serial section array SEM (Reichelt et al., 2012) and serial section scanning electron microscopy (ssSEM or S^{3}EM, Horstmann et al., 2012).

A substantial improvement for ssTEM imaging was achieved by Bock et al. (2011) who increased the acquisition rate by an order of magnitude by introducing a high-throughput TEM camera array and fast stage motion control to move between frames. Automatic section collection for ssTEM is under development (Hess et al., 2015, US Patent Application 20150135917, 'Sectioning Volume Samples'), but not yet available for general use.

Besides automation, two other factors were crucial for the recent advances in volume (S)EM: (1) Remarkable improvements in storage capacity and processing power over the past 20 years have made it possible to rapidly store and manipulate vast amounts of image data. All techniques described above acquire digital image stacks and rely on various software tools and powerful computer hardware for processing them. (2) A new generation of SEMs has boosted pixel acquisition rates by offering higher beam currents at low beam energies, larger fields of view and more sensitive and faster signal detection systems.

Serial section versus serial block-face techniques

With serial section techniques (ssTEM, ssSEM/Array Tomography, ATUM-SEM), the sample is cut into consecutive thin sections before the imaging process begins. All sections are preserved and can be (re)imaged multiple times. With serial block-face techniques (SBEM and FIB-SEM), all images are acquired from the surface of a sample block. The imaging is tied to the cutting or milling process: After each abrasion, the freshly exposed surface must be imaged before the next slice is cut or milled off. The removed material is lost.

In the following, we will describe SBEM, FIB-SEM and ATUM-SEM in detail. These three methods have in common that they use scanning instead of transmission EM, offer a high level of automation and are available commercially.

Serial block-face electron microscopy

A SBEM system consists of a scanning electron microscope, a diamond-knife microtome mounted on the inner side of the microscope's vacuum chamber door (Figures 1a and 1b) and additional hardware and

Figure 1 | Serial block-face electron microscopy (SBEM) (a) SBEM microtome attached to the inner side of the SEM vacuum chamber door. Knife holder and sample visible in red rectangle. Y-motor hidden from view. (b) Close-up view of the knife holder and the mounted sample. 1: Rear end of the diamond knife. The knife is clamped in the metal holder, its front part and blade hidden from view. 2: Piezo actuator used to oscillate the knife perpendicular to the cutting direction. (c) View from above through a light microscope. Diamond knife and sample positioned for a cut. Crumpled cut-off slices are visible on the knife's blade.

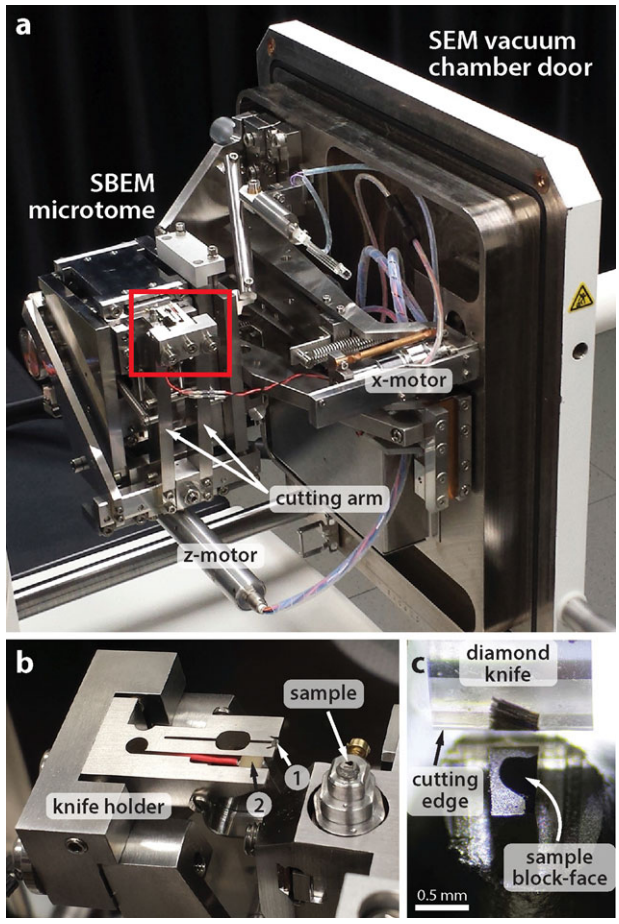

software to control the acquisition process (Denk and Horstmann, 2004). The user inserts the sample into the SBEM microtome holder and carries out a manual approach procedure to move the sample surface up until it reaches the level of the knife's cutting edge. Then, the SEM chamber is evacuated, the imaging parameters are set and the automatic acquisition begins. Each time the region of interest on the sample

surface has been imaged, the sample is moved up by the desired slice thickness (usually set to 25–200 nm) and the knife removes the entire surface of the block-face (Figure 1c). After each cut, the region of interest is imaged on the freshly exposed surface. This cut-and-image cycle can run continuously, acquiring thousands of serial images without user interaction.

A sharpened and intact knife blade is critical to achieve uniform slice thickness and avoid cutting artefacts. Oscillating the knife laterally (Studer and Gnaegi, 2000) may improve cutting quality. Slice thicknesses well below 25 nm are mechanically possible (Hashimoto et al., 2016), but electron dose restrictions for cutting resin-embedded biological samples make routine use of <25 nm thickness difficult (discussed further below).

'Tiling' is required if the region of interest on the block-face is larger than the SEM's field of view (FOV: maximum image size for given imaging parameters). A mosaic of overlapping image tiles covering the region of interest is acquired by moving the sample laterally on a motorised SBEM stage (Briggman et al., 2011). A recent approach to speed up tiled acquisitions is 'continuous line scanning' (Kevin Boergens, MPI for Brain Research, personal communication): Here, the SEM is continuously acquiring a single line in the x-direction while the sample is being continuously moved in the perpendicular y-direction, thus generating a long rectangular image. This saves time, since stage moves between tiles are no longer necessary in the y-direction.

Cut-off slices usually stick to the knife and pile up on its blade (Figure 1c). Occasionally, these slices or pieces of them ('debris') fall onto the sample where they may obscure the region of interest. Low-resolution overview images can be automatically inspected before the region of interest is captured at full resolution. If debris is detected, a 'sweep' is performed: The knife is moved across the sample closely above its surface (e.g. 40 nm) to push the debris away (Helmstaedter et al., 2013).

Focus and astigmatism drifts that compromise image quality may occur when a SBEM system is continuously operating for weeks or months (as in Briggman et al., 2011). While manual adjustments are possible by repeatedly pausing the acquisition and refocusing, more effective algorithmic solutions have been developed that allow automatic correction (Binding et al., 2013; various algorithms in commercial software).

Resin-embedded stained biological tissue is poorly conducting and thus prone to charging effects when imaged with an SEM. Accumulation of negative surface charge causes image distortions and irregular contrast. This is a common problem for SBEM imaging, but it may also occur for other types of volume SEM to various degrees, depending on how much conductivity is provided by heavy-metal staining (see Section Sample Preparation). There are several approaches to eliminate or minimise charging: (1) Re-embedding the sample in a surrounding conductive medium, for example silver epoxy (Wanner et al., 2016) or resins containing carbon-based fillers (Nguyen et al., 2016). (2) Introduction of a gas, for example water vapour, into the vacuum chamber – a widely used method called low-vacuum, environmental, or variable-pressure SEM (Robinson, 1975; Moncrieff et al., 1978). (3) Cyclical (re)coating of the sample surface inside the vacuum chamber during a SBEM acquisition (Titze and Denk, 2013).

Commercial development of SBEM began soon after its invention. 3View, based on the original design described in Denk and Horstmann (2004), is a commercial SBEM system produced by Gatan, available for SEMs by ZEISS, FEI, JEOL and TESCAN. Besides biological applications, 3View is increasingly used for materials science (Zankel et al., 2014). Another commercial SBEM system is Teneo VS (VolumeScope), recently introduced by FEI. It employs multi-energy deconvolution (Lich et al., 2013) to obtain higher z-resolution: After each cut with a diamond knife, the surface is imaged multiple times at increasing beam energy. Depth information is then computationally reconstructed from the image series. Combining 50-nm physical slicing with 10-nm 'virtual slicing' (five images per slice, followed by deconvolution) allows volume acquisitions at 10 nm isotropic voxel size (Matthias Wolf, OIST, personal communication).

Focused ion beam scanning electron microscopy

FIB systems for milling and nanofabrication appeared in the 1980s and quickly became routine technologies in the semiconductor industry and for materials science. The main components of a FIB system are a vacuum chamber, a liquid metal ion source and an ion column, which accelerates and focuses the ions (Giannuzzi and Stevie, 2005). FIBs can either

Figure 2 | Focused ion beam scanning electron microscopy (FIB-SEM)
(a) FIB-SEM system. The gallium ion gun is mounted on the SEM vacuum chamber at an angle of usually 52° or 54°. (A 90° configuration was recently introduced by Hitachi.) (b) The electron beam and the ion beam coincide in the vacuum chamber. (c) The focused ion beam moving across the sample surface milling away a thin layer. Image adapted from Knott et al. (2008), used with permission.

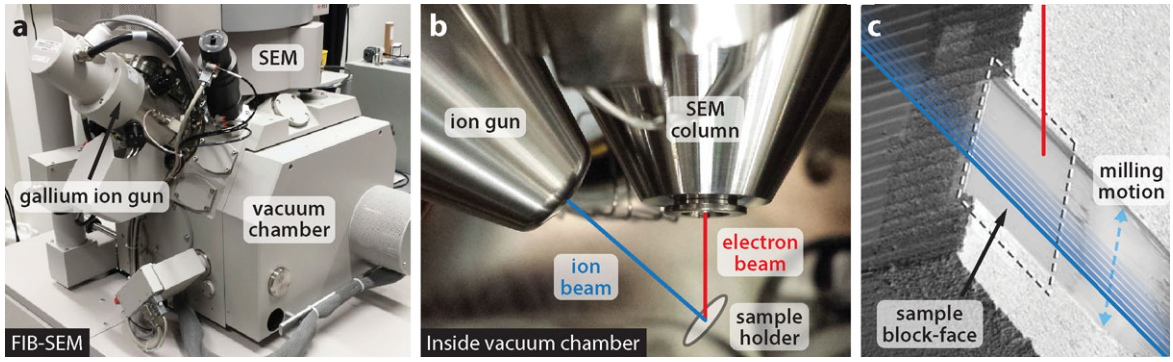

remove material by bombardment of the surface with high-energy ions, or assist in the deposition of materials (e.g. carbon or platinum) onto surfaces. The high precision with which a beam of ions can be used to manipulate surfaces led to the production of microscopes that combined a scanning ion beam with a scanning electron beam (FIB-SEM; Figures 2a and 2b).

It was not until the end of the 20th century that the possibilities of FIB-SEM for biology were recognised (Ballerini et al., 1997). A beam of gallium ions accelerated with a voltage of 30 kV was then shown to be capable of iteratively milling a small region of a resin-embedded tissue sample (Figure 2c), from which serial electron micrographs could be captured (Heymann et al., 2006; Knott et al., 2008). Analogous to SBEM, the freshly exposed sample surface – polished by the ion beam – is imaged after each milling cycle. Besides the advantage of full automation, the FIB's capability to reliably remove as little as a few nanometres after each image lets users collect image series with isotropic voxels down to 3–5 nm voxel size (Wei et al., 2012). This level of resolution in 3D is sufficient to visualise all organelles and large macromolecular complexes, which has made FIB-SEM a powerful tool for biological research (for an in-depth primer, see Narayan and Subramaniam (2015); for detailed workflow descriptions, see Bushby et al. (2011), Knott et al. (2011) and Maco et al. (2014)).

The part of the ion beam that passes the sample surface can be automatically monitored to maintain consistent FIB-SEM slice thickness during acquisitions (Boergens and Denk, 2013). This makes the system more robust against temperature fluctuations and also allows an acquisition to be stopped and restarted seamlessly, for example when the ion gun needs to be reheated, or 'reconditioned', to allow the nozzle of the ion source to be cleaned.

While FIB-SEM's lateral resolution is lower than that of (ss)TEM, it is the only technique with the capability to routinely collect serial images at 5 nm isotropic voxel size over FOVs of tens of micrometres. There are limitations, however, to the ion beam's milling accuracy over large areas. Artefacts are caused by curtaining (non-planar milling) and by redeposition of vaporised material. The wider the milled face, the greater the amount of time needed for milling and the less focused the beam at the widest extent of its scanning arc. Also, as the ions interact with the sample surface along the beam direction, the energy with which they can vaporise material diminishes. This reduces the milling efficiency and eventually causes vaporised material to accumulate and obscure the imaging. This process of redeposition will also occur at the edges of the milled face, which risks obscuring the imaging window.

These restrictions limit the width of the surface that can be acquired to about 20 μm when highest milling precision is required, which has driven

researchers to explore other methods when FIB-SEM is needed for imaging large volumes, for example neuronal circuits. Hayworth et al. (2015) have elegantly demonstrated that a single resin-embedded block of tissue can be cleanly cut in two using a heated ultrasonic diamond knife. The two halves can be milled and the resulting images matched together with sufficient precision to trace thin neuronal processes across the cut.

ATUM-SEM imaging

ATUM-SEM (Hayworth et al., 2006; Schalek et al., 2011, 2012), a serial section technique, offers automated ultrathin section cutting and collection, followed by semi-automated high-throughput SEM imaging. To acquire a volume with ATUM-SEM, the first step is to mount the sample in an ultramicrotome equipped with a diamond knife that is attached to a water-filled boat. Consecutive thin sections (thickness typically ~30 nm) are cut off the sample block and floated onto the water surface. A sharpened and intact knife blade is crucial for high-quality uniform sectioning. After about 5000 cuts, the sample should be shifted relative to the knife, so that cutting can be continued with a fresh part of the blade (Richard Schalek, Harvard, personal communication). An automated water filling mechanism keeps the knife wet, which allows unattended sectioning for days.

The ATUM device, attached to the front of the ultramicrotome, automatically collects the floating sections onto a continuous 8-mm-wide tape, which is supplied by a computer-controlled reel-to-reel conveyer belt mechanism (Figures 3a and 3b). Kapton, a polyimide, is the primary tape material used (50 μm tape thickness), polyether-ether-ketone an alternative; lumox and polycarbonate film may be used for studies combining light and SEM imaging (R. Schalek, personal communication). Thousands of consecutive sections can be collected onto the tape. They adhere to it, allowing the section-carrying tape to be wound up on a reel (Figure 3c). The ATUM tape provides higher stability compared to TEM grids or support films, but it is not transparent for an electron beam and therefore TEM imaging is not possible.

To prepare the sections for imaging in an SEM, the tape holding the sections is cut into strips. These are mounted with double-sided conductive tape onto silicon wafers (Figure 3d). These wafers (diameter: 100 mm) collectively form a 'section library' (Figure 3e) of the tissue volume. Sections on wafers can be post-processed (e.g. immunostaining) and imaged multiple times at different imaging parameters. They can be stored for long periods of time in a clean and dry space. After 5 years, it was found that virgin section regions showed little or no image degradation, and previously imaged regions showed moderate image degradation, but tolerable for neuronal circuit reconstruction (R. Schalek, personal communication).

For imaging, the wafers holding the sections are individually placed into an SEM. The software tool WaferMapper was developed to direct the acquisition process of selected sections from the library (Hayworth et al., 2014). Commercial imaging software can also be used (Atlas 5 Array Tomography, ZEISS). Backscattered or secondary electrons (especially for high-speed imaging at up to 20 MHz) are used for image acquisition. Lateral pixel sizes of 3–4 nm have been reported for large-scale acquisitions (Kasthuri et al., 2015; Morgan et al., 2016). The maximum section size is limited by the width of the diamond knife (4 mm) and the reliability of the cutting process. Sections as large as 3 mm × 3 mm can be reliably cut, which lets users image very large regions of interest using tiling.

The ATUM was recently commercialised under the name ATUMtome (RMC Boeckeler product line by Boeckeler Instruments). It can be combined with commercial diamond-knife ultramicrotomes and SEMs from different manufacturers. The cutting of the tape, its transfer onto the wafers and the repeated transfer of wafers into the SEM must be carried out manually at this point, but full automation appears feasible.

Choosing the right tool for the job

We will now compare the three techniques presented above and discuss their respective strengths and weaknesses. Which technique to choose for a given application mainly depends – apart from instrument availability – on the size of the target volume, the required lateral (x, y) and z-axis resolution, whether sections need to be retained, and on the amount of time available for the acquisition.

All three techniques – SBEM, FIB-SEM and ATUM-SEM – achieve better z-resolution in routine

Figure 3 | Automated tape-collecting ultramicrotome (ATUM)
(a) ATUMtome full view. (b) Close-up view of the tape collection mechanism. The cutting arm moves the sample vertically, causing ultrathin sections to be cut off by the stationary diamond knife. The sections are picked up from the water surface onto the tape, which moves like a conveyor belt in the direction indicated by the dashed arrow. The water level in the blue boat is maintained automatically. (c) The tape after section collection is completed. (d) A wafer populated with sections on strips of tape, ready for imaging in an SEM. (e) Ultrathin section library consisting of numerous populated wafers. Images in panels (a) and (b) courtesy of Boeckeler Instruments, Inc. Images in panels (c)–(e) reproduced under Creative Commons Licence BY 3.0 from Hayworth et al. (2014).

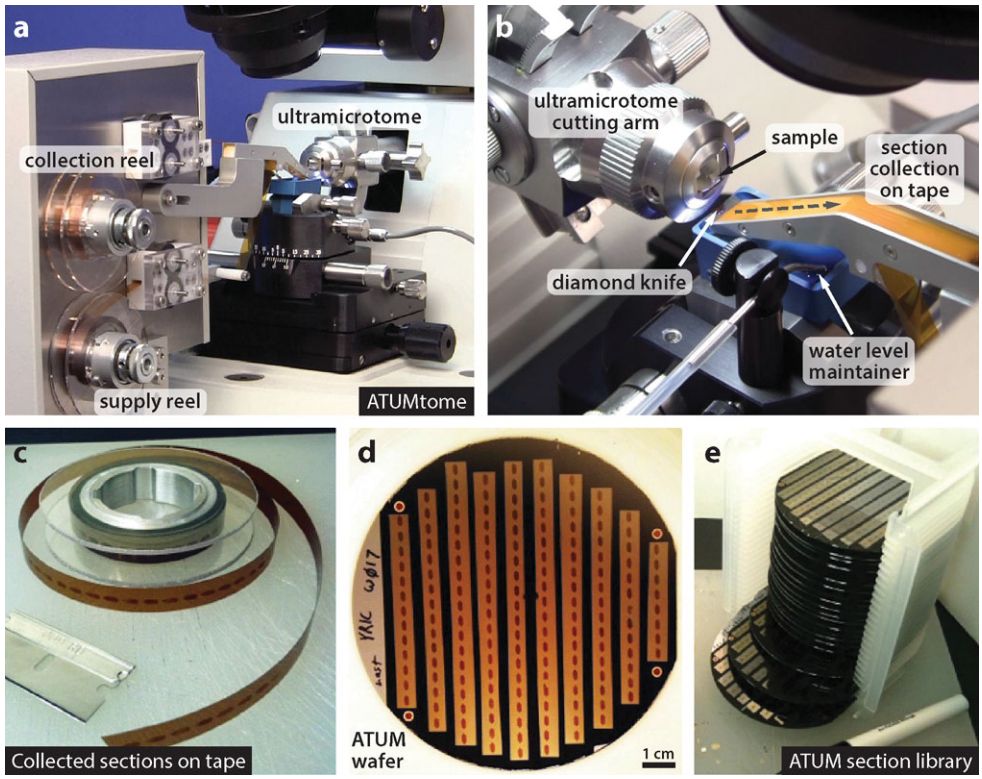

use than manual ssTEM, for which a section thickness of 40–50 nm is the limit (Harris et al., 2006; Bock et al., 2011; Lee et al., 2016). State-of-the-art voxel sizes are $10 \times 10 \times 25$ nm^3 for SBEM (Wanner et al., 2016), $5 \times 5 \times 5$ nm^3 for FIB-SEM (Knott et al., 2011; Boergens and Denk, 2013) and $3 \times 3 \times 30$ nm^3 for ATUM-SEM (Kasthuri et al., 2015).

SBEM and FIB-SEM offer several advantages over manual ssTEM and ATUM-SEM: (1) SBEM/FIB-SEM images are inherently aligned since they are acquired from a rigid block-face. Small amounts of jitter can be neglected or easily corrected. (2) No sections must be handled for SBEM and FIB-SEM. ATUM's sectioning process is a significant improvement over manual ssTEM, but it still comes with a risk of occasionally damaging or losing sections. (3) Wrinkles, folds and distortions of ATUM-SEM or ssTEM images pose a greater challenge for image registration. (4) SBEM and FIB-SEM provide a fully automated acquisition cycle, which reduces manual labour to a minimum.

ATUM-SEM, on the other hand, offers more flexibility than SBEM and FIB-SEM because it preserves all sections. The separation of section collection from the imaging process is a crucial advantage for several scenarios: (1) Screening the section library before selectively imaging subvolumes at higher resolution, (2) post-staining or labelling the sections, or manipulating them in other ways, (3) (re)imaging sections at any time ('random access'),

choosing multiple regions of interest and using different imaging conditions or other imaging modes such as light microscopy, and (4) parallelisation of the imaging workload on multiple SEMs for very large volumes.

A specific weakness of SBEM is the sensitivity of diamond-knife cutting to the electron dose for resin-embedded biological samples (Titze, 2013; Kubota, 2015). The electron dose is defined as the number of beam electrons hitting the sample surface per unit area. Increasing the dose yields better image quality (higher signal-to-noise ratio), but adversely affects thin cutting (10–30 nm thickness): If the dose is too high, cutting becomes non-uniform (varying slice thickness, skipped or partial cuts). FIB milling is less sensitive in that regard, and ATUM-SEM's sectioning process is independent of imaging. Therefore, FIB-SEM and ATUM-SEM permit users to choose higher lateral resolutions, higher beam currents and longer pixel dwell times, which all increase the electron dose.

The maximum sample width is determined by the knife width for SBEM (1.5 mm for 3View knives; Diatome), ion gun milling constraints for FIB-SEM (maximum FOV is $\sim$20 μm for highest milling precision, otherwise up to 100 μm) and the knife width and the reliability of section collection for ATUM-SEM (maximum width: $\sim$3 mm). The z-depth of a continuous acquisition is limited by the z-stage range for SBEM (up to about 700 μm) and the ion gun z-range for FIB-SEM. The ATUM's z-depth is limited by the maximum range of the ultramicrotome's cutting arm travel (usually 100–200 μm). At the end of the range, the user must perform a manual reset, which interrupts the sectioning process and leads to the temporary collection of partial sections when cutting is resumed.

The total duration of a SBEM or FIB-SEM acquisition is the sum of (1) the cutting or milling time, (2) the raw imaging time for all image tiles and (3) the time needed for lateral stage moves between tiles, including waiting times to let vibrations subside after moves. For ATUM-SEM acquisitions, the durations of the following steps must be added: (1) section collection on tape, (2) manual wafer preparation, (3) wafer mapping (optical or SEM imaging) and (4) wafer imaging at target resolution (manual preparation/setup times, raw imaging time and stage movements).

Table 1 provides a summarised comparison of SBEM, FIB-SEM and ATUM-SEM. Estimates for durations and dataset sizes for the acquisition of example volumes are also listed. A side-by-side comparison of example images (x–y planes and z-reslices) can be found in Briggman and Bock (2012).

For a given application, the above considerations will allow users to decide on the most suitable technique. For acquiring small volumes at the highest possible isotropic resolution, FIB-SEM is clearly the best and currently only choice. For volumes ranging from small to large, SBEM offers a good compromise of voxel size, speed and ease of use. ATUM-SEM is the most challenging technique from a user perspective, and at this point requires large amounts of manual labour. It is best suited for medium to very large acquisitions, especially when exploiting its advantage of preserving sections.

Turning tissue into data: the volume SEM workflow

Sample preparation

The crucial first step, which takes about 5 days for most applications, is sample preparation (Figure 4, left column). EM imaging requires special preparation techniques (Hayat, 2000): The sample must (1) withstand the vacuum and the high energy and current of the electron beam, (2) deliver sufficient image contrast and (3) exhibit sufficient structural rigidity, especially for volume slicing. A suitable sample preparation should preserve the ultrastructure in a state as close as possible to the *in vivo* state. In the following, we will summarise the standard sample preparation pipeline for volume SEM and highlight specific requirements for SBEM, FIB-SEM and ATUM-SEM.

After dissection, the tissue is fixed. Usually, a chemical fixation is performed with a mixture of 2–4% paraformaldehyde and 1–4% glutaraldehyde, which is an effective method to preserve the tissue's ultrastructure. Cryofixation has been shown to reduce fixation artefacts compared to chemical fixation for FIB-SEM (Korogod et al., 2015). Preserving extracellular space is advantageous for reconstructing neuronal circuits in SBEM datasets (Pallotto et al., 2015).

Fixation is followed by staining. Heavy metals such as osmium, lead and uranium are commonly used. They provide contrast for SEM imaging and

Table 1 | Comparison of volume SEM techniques

	SBEM	FIB-SEM	ATUM-SEM
Fully automated acquisition **(note 1)**	Yes	Yes	No
Sections preserved for post-processing and "random-access" imaging	No	No	Yes
State-of-the-art voxel size (x, y, z)	10 × 10 × 25 nm^3 **(note 2)**	5 × 5 × 5 nm^3	3 × 3 × 30 nm^3
Maximum slice/milling/section width	~1 mm	~20–100 μm **(note 3)**	~3 mm
Problems specific to each technique	Slice debris, surface charging, sensitivity to electron dose	Redeposition of vaporised material	Wrinkled sections, occasional section damage or loss
Staining	only *en bloc*	only *en bloc*	*en bloc* or section staining
Stitching and alignment	Translational shifts usually sufficient	Translational shifts usually sufficient	Demanding because of distortions and rotations
Acquisition time estimates and dataset sizes for example volumes **(note 4)**			
10 × 10 × 10 μm^3	2 h; 0.4 GB	39 h; 8 GB	23 h; 3.7 GB
20 × 20 × 20 μm^3	4 h; 3.2 GB	10 days; 64 GB	2 days; 30 GB
50 × 50 × 50 μm^3	22 h; 50 GB	4 months; 1 TB	6 days; 460 GB
100 × 100 × 100 μm^3	5 days; 400 GB	–	15 days; 3.7 TB
200 × 200 × 200 μm^3	5 weeks; 3.2 TB	–	8 weeks; 30 TB
1000 × 1000 × 1000 μm^3 (= 1 mm^3)	13 years; 400 TB	–	12 years; 3700 TB

Note 1: After mounting sample until acquisition of image stack completed. **Note 2**: 10–15 nm slice thickness possible for some samples when electron dose kept low enough (Sarah Mikula, personal communication; 15 nm advertised as minimum slice thickness for Gatan 3View); <10 nm lateral pixel size possible if slice thickness increased. 10 nm isotropic pixel size attainable with FEI Teneo VS, but multiple images per slice and deconvolution required. **Note 3**: Limit is ~20 μm when highest milling precision required (Maco et al., 2014). **Note 4**: Storage size calculations (figures rounded) assume 1 byte/voxel; overlapping voxels are not included. Duration estimates (figures rounded) based on the following assumptions: Voxel size for each technique as listed above in the table. SBEM: 1 MHz effective pixel acquisition rate (includes overhead for tiling), cutting time: 15 s per slice. FIB-SEM: 0.1 MHz pixel rate; milling times: 30 s per cycle (10 μm), 60 s (20 μm) and 150 s (50 μm). ATUM-SEM estimates based on Hayworth et al. (2014) and personal communication (Richard Schalek): Section collection rate: 10 s per section. Wafer preparation (200 sections per wafer): 30 min per wafer, maximum 20 wafers per day. (Optical) wafer mapping: 2 h per wafer, maximum 5 wafers per day. Loading and setup procedure for imaging: 20 min per wafer. Stage correction and focusing: 3 min per section; 10 MHz effective pixel rate (high-speed secondary electron imaging; rate includes tiling overhead).

also increase sample conductivity, thereby minimising charging. For ATUM-SEM, sections may be counterstained on the wafers (Kasthuri et al., 2015). SBEM and FIB-SEM samples must be stained *en bloc*.

A common method to stain biological specimens *en bloc* is the rOTO protocol (rOTO: reduced osmium – thiocarbohydrazide – osmium), developed several decades ago (Seligman et al., 1966; Malick et al., 1975; Willingham and Rutherford, 1984). Recent adaptations for volume SEM include Deerinck et al. (2010), Starborg et al. (2013) and Hua et al. (2015), and an OTO variant reported by Tapia et al. (2012). The osmium steps can be followed by additional staining with uranyl acetate and lead aspartate to further increase heavy-metal content and thereby improve image contrast. Penetration depth for heavy-metal *en bloc* staining is typically limited to much below a millimetre, but significant advances have recently been reported for staining very large volumes such as whole mouse brains (Mikula et al., 2012; Mikula and Denk, 2015).

The staining protocol is followed by a graded ethanol or acetone series to replace all remaining water in the sample. Next, the sample is embedded in epoxy resin, which replaces the ethanol or acetone. Common choices for epoxy resins are Epon 812 substitutes, Spurr's (Spurr, 1969) and Durcupan (Stäubli, 1963), which provide sufficient sample penetration as well as stability during electron beam irradiation and cutting with a diamond knife. The formulations 'Hard Plus' and a mixture of Durcupan/Epon were recently shown to be most suitable for FIB-SEM (Kizilyaprak et al., 2015).

Figure 4 | Volume SEM workflow from tissue to dataset

Left column: Visual summary of the sample preparation process. Middle column: Simplified schematic illustrations of the SBEM, FIB-SEM and ATUM-SEM acquisition process (not to scale). Right column: The acquired images are transformed into a 3D representation of the volume that can be annotated and analysed.

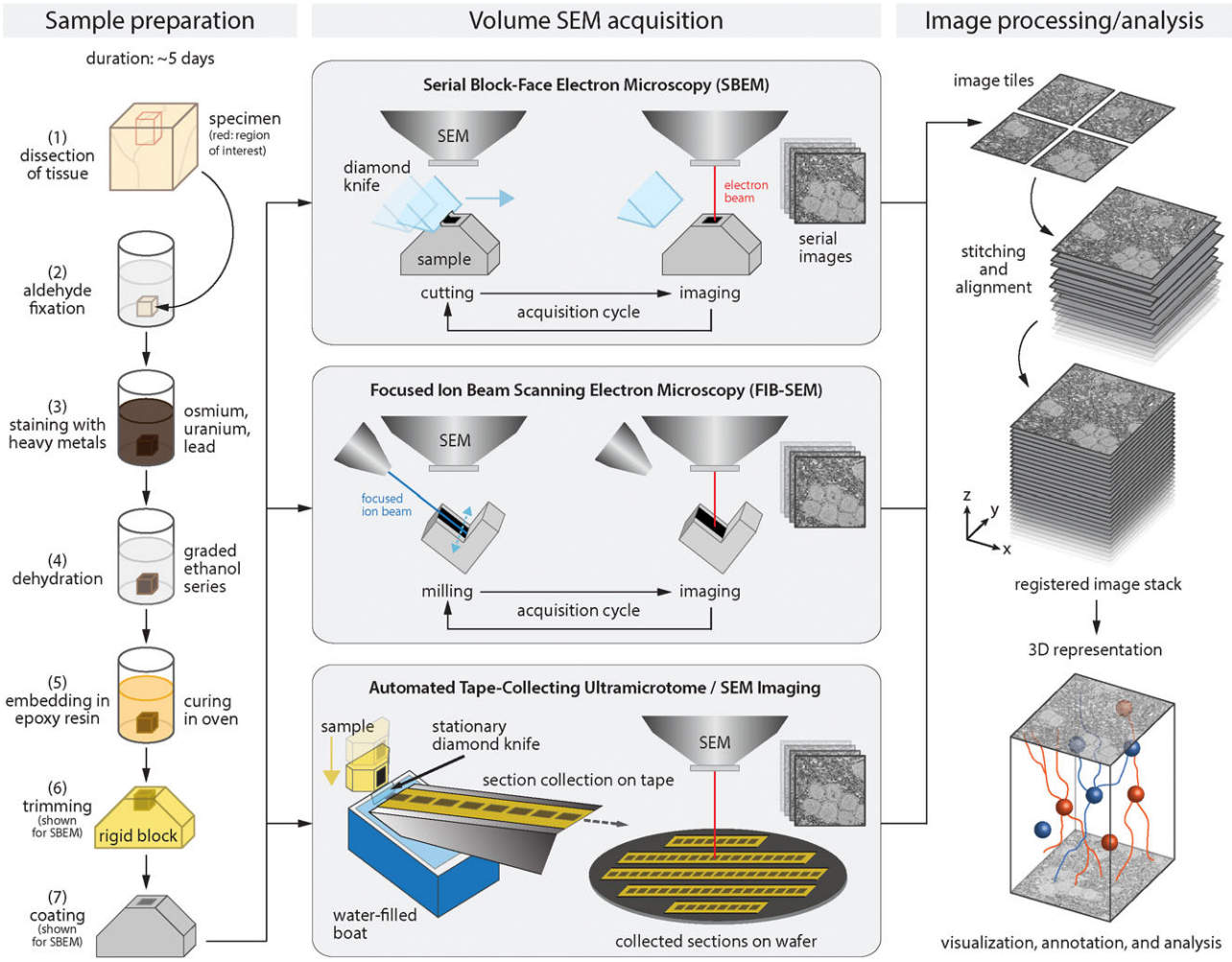

High-quality sample preparation is an essential requirement for successful volume SEM acquisitions. Obtaining good tissue preservation and staining quality for a given specimen is often a major obstacle or even the biggest challenge. Testing and optimising different protocols is time-consuming, but often unavoidable.

Volume SEM offers a fresh look at ultrastructure in three dimensions, which can reveal anatomical features that could not be inferred from single 2D images. However, EM sample preparation introduces various artefacts. For example, staining may be highly selective for certain biological structures and may mask subtle features of other structures. Therefore, caution should be applied when drawing conclusions from studies using a single method of sample preparation.

Trimming, coating and mounting the sample

The stained and embedded sample must be trimmed (with a razor blade, a milling system or a microtome) to a size and shape that allows it to be mounted in a SBEM or FIB-SEM system, or in a commercial ultramicrotome for ATUM sectioning. For SBEM, the sample is usually trimmed to a truncated pyramidal shape centred on the region of interest (Figure 4,

bottom left). Before transferring the sample into the SEM chamber, it can be coated with a metallic layer (e.g. gold) to allow negative charge to drain more easily and thus prevent charging. For FIB-SEM, the smoothed sample surface of the area to be milled is positioned perpendicular to the ion beam and coated with a 1-μm protective layer of carbon or platinum (Bushby et al., 2011; Knott et al., 2011).

For ATUM-SEM, a variety of block-face shapes are possible as long as each section pushes the previous one off the knife edge during continuous sectioning. For secondary electron imaging, the tape is coated with carbon or indium tin oxide before section collection to make it conductive. For backscattered electron imaging, a carbon film is deposited onto the sections after they have been collected on uncoated tape (Hayworth et al., 2014).

Volume SEM acquisition

A SBEM/FIB-SEM acquisition (Figure 4, middle column, upper two panels) can start after the sample has been mounted and the SEM chamber pumped to high or variable-pressure vacuum conditions. Controlled by custom-written software (Briggman et al., 2011; SBEMimage, B. Titze, unpublished) or commercial software (e.g. DigitalMicrograph for 3View), the acquisition may run without any or minimal user interaction. For ATUM-SEM (Figure 4, middle column, bottom panel), the sample is mounted in the ATUM(tome), which automatically cuts the sections and collects them on tape. The tape is manually cut and transferred onto wafers, which are inserted into the SEM for imaging using the software WaferMapper (Hayworth et al., 2014).

To achieve the target resolution and an adequate signal-to-noise ratio for the intended application, appropriate SEM imaging parameters must be chosen (see Goldstein et al., 2003, for an introduction). For SBEM and ATUM-SEM, pixel acquisition rates in the megahertz range can be achieved with state-of-the-art SEMs and signal detection systems for both backscattered and secondary electrons (Titze and Denk, 2013; Hayworth et al., 2014). For FIB-SEM, typical pixel acquisition rates are around 100 kHz (Knott et al., 2011). For SBEM and FIB-SEM, electron beam energies must be adjusted within a range of typically 1–3 keV to ensure that the depth of the backscattered electron signal (Hennig and Denk, 2007) matches the slicing or milling thickness.

From image stacks to analysable datasets

A volume SEM acquisition results in a collection of consecutive digital images (Figure 4, right column). To obtain a 3D representation, these images must be accurately positioned in a virtual volume. This process, called 'registration', is easiest for single-tile SBEM/FIB-SEM stacks (one image per slice), since distortions are usually negligible and small amounts of lateral displacements ('jitter') between consecutive images can be corrected with 2D registration algorithms (Guizar-Sicairos et al., 2008). For multi-tile SBEM stacks, more effort is required. The overlapping tiles of the mosaic must be joined together ('stitched') to form a continuous image (further explained and illustrated in Wanner et al., 2015). ATUM-SEM stacks require more advanced algorithms for stitching and alignment to correct rotations and (non-linear) distortions. Free and open-source registration tools include Fiji (Schindelin et al., 2012), a distribution of ImageJ that contains TrakEM2 (Cardona et al., 2012; Saalfeld et al., 2012) and the large-scale EM Aligner developed at HHMI/Janelia Research Campus (Scheffer et al., 2013).

Following registration, the 3D dataset can be explored and analysed with a variety of tools that offer digital reconstruction (e.g. tracing morphology to capture cellular and subcellular structures), visualisation and annotation. Besides commercial software such as Amira or Imaris, free tools are available, for example KNOSSOS (Helmstaedter et al., 2011), TrakEM2 (Cardona et al., 2012), CATMAID (Saalfeld et al., 2009; Schneider-Mizell et al., 2016), ilastik (Sommer et al., 2011), Microscopy Image Browser (Belevich et al., 2016) or VAST (Kasthuri et al., 2015). A literature survey of volume EM data processing tools has recently been conducted (Borrett and Hughes, 2016); a more comprehensive list of software tools can be found there.

One can distinguish between sparse and dense reconstruction approaches: For a dense reconstruction, the aim is to capture all visible structures of the acquired volume, whereas a sparse reconstruction targets a small subset. Since the time needed to digitally reconstruct a tissue volume is usually much longer than the time needed to acquire it, one must carefully set realistic goals for reconstruction efforts, since (semi-)automated reconstruction tools are not yet ready for routine use and manual

Figure 5 | Examples of biological ultrastructure imaged with SBEM and FIB-SEM

(a) SBEM reconstruction of the bloodstream form of *Trypanosoma brucei*, a parasitic protozoan. Top left: a single slice from the SBEM dataset. Right and bottom: Volume renderings. Scale bar: 500 nm. Reproduced with permission from Gluenz et al. (2015). (b) Cross-sections of a *C. elegans* head (adult hermaphrodite). Dataset acquired with SBEM. Scale bar: 10 μm (www.wormatlas.org). Raw data provided by Joel Mancuso, Gatan. Reproduced with permission. (c) Dense reconstruction of 950 neurons in a tissue volume of mouse retina acquired with SBEM. Dimensions: 132 $\times$ 114 $\times$ 80 μm^3. Voxel size: 16.5 $\times$ 16.5 $\times$ 25 nm. Illustration © Fabian Isensee, Julia Kuhl; Helmstaedter et al. (2013); MPI for Medical Research, Heidelberg, Germany. Reproduced with permission. (d) A yeast cell reconstructed from an anisotropic FIB-SEM dataset (4 $\times$ 4 $\times$ 15 nm^3), showing the endoplasmic reticulum (yellow), the nucleus (light blue), mitochondria (red), cisternae (green), vesicles (light green), lipid droplets (orange), microtubules (pink) and the cell wall (grey). Reproduced with permission from Wei et al. (2012). (e) Mouse neural tissue acquired with FIB-SEM at 5 nm isotropic voxel size. Scale bar: 500 nm. Courtesy of G. Knott, EPFL. (f) A cultured cell acquired with FIB-SEM. Courtesy of Anna Steyer, Schwab team, EMBL Heidelberg.

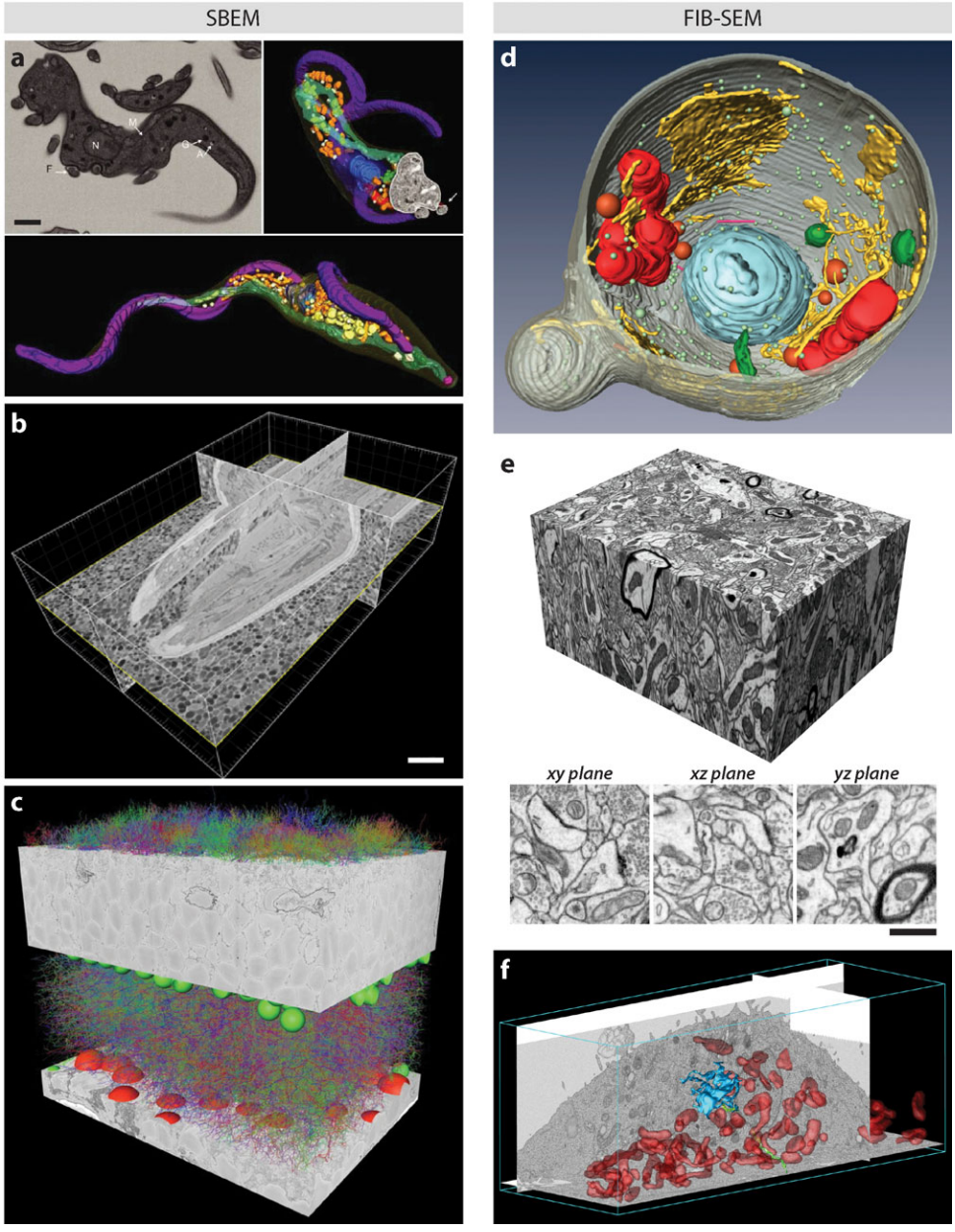

reconstruction is often the only option (Peddie and Collinson, 2014).

Large-scale mapping of neuronal circuits ('connectomics') is currently by far the most demanding application for volume EM. Discussing the specific challenges of data processing, reconstruction and analysis for connectomics is beyond the scope of this review; for further reading, we recommend Lichtman and Denk (2011), Denk et al. (2012), Helmstaedter and Mitra (2012), Helmstaedter (2013) and Plaza et al. (2014).

Cells, tissues and neuronal networks

Neuronal circuit reconstruction propelled the development of volume EM techniques (Briggman and Denk, 2006; Smith, 2007), but the new possibilities they offer extend to other biological applications. In the field of cell and tissue biology, a large number of studies in recent years have used SBEM or FIB-SEM to characterise organelles and perform quantitative structural analysis in cell cultures and tissues. A compilation and detailed discussion of such studies is provided in Peddie and Collinson (2014). The potential of FIB-SEM for imaging biological ultrastructure in the native state was recently shown by Schertel et al. (2013), who milled and imaged mouse optic nerves and *Bacillus subtilis* spores at cryo temperatures. ATUM-SEM was used for investigating the 3D nanostructure of the endoplasmic reticulum in neuronal and secretory salivary gland cells (Terasaki et al., 2013).

Since knowledge of structure alone is often insufficient to understand biological systems, experiments probing tissue function *in vivo*, for example with light microscopy, are essential to complement ultrastructural investigations. Volume SEM is well suited to complement *in vivo* light imaging on the same sample (Peddie and Collinson, 2014), as shown for the combination of two-photon microscopy (Denk et al., 1990) with SBEM (Briggman et al., 2011) and with FIB-SEM (Maco et al., 2013). A variety of biological specimens imaged with SBEM and FIB-SEM, and approaches to combine light microscopy with volume SEM are presented in Kremer et al. (2015). Correlative imaging with confocal light microscopy and SBEM was recently demonstrated by Bohórquez et al. (2015).

Figure 6 | ATUM-SEM application examples

(a) Helicoidal membrane motifs connecting stacked endoplasmic reticulum (ER) sheets, discovered in a dataset acquired with ATUM-SEM. Scale bar: 200 nm. The stacked ER sheets resemble a parking garage with ramps connecting different levels (Terasaki et al., 2013). Reproduced with permission. (b) Reconstructed neuronal tissue from an ATUM-SEM dataset of mouse neocortex. The region marked with a pink arrow was densely reconstructed. A selection of reconstructed cell types is shown in the bottom panel (scale bar: 5 μm). Reproduced with permission from Kasthuri et al. (2015).

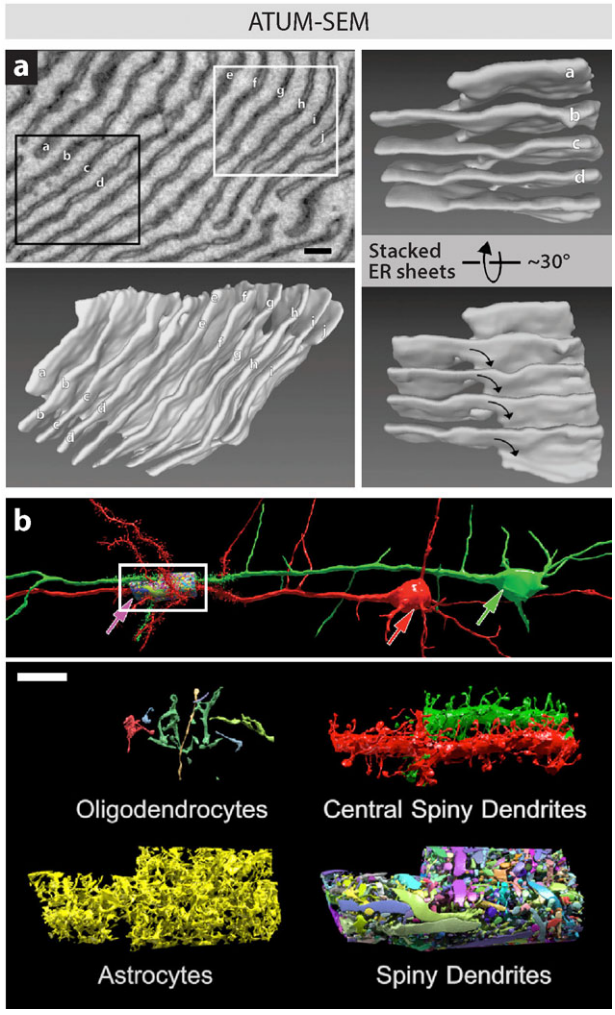

In Figure 5, we show several examples of volume SEM data and renderings of reconstructed tissue to illustrate the capabilities of SBEM and FIB-SEM. In Figure 6, we highlight two studies using ATUM-SEM.

Conclusions and outlook

Automated volume SEM techniques have substantially improved the acquisition of biological tissue in three dimensions with regard to reliability, z-resolution and speed. The availability of commercial versions for the three techniques discussed in detail in this review – SBEM, FIB-SEM and ATUM-SEM – extends their use for biological research beyond the pioneering laboratories. Increased availability of these techniques in central EM facilities will also expand their user base.

For large-scale studies, especially in the field of neuroscience, the current limits of sample size and acquisition speed will continue to be pushed. Moving towards bigger volumes will depend on achieving reliable diamond-knife cutting of large surfaces (Marx, 2012) or losslessly dividing samples for parallel processing (Hayworth et al., 2015). Surface ablation with laser light may be an alternative approach (Kanemaru and Oki, 2015). To boost acquisition speed, ZEISS has recently introduced a new type of SEM featuring a column with 61 electron beams (Eberle et al., 2015; 91 beams in a newer version, Kemen et al., 2015). This multi-beam SEM ('MultiSEM') can simultaneously image 91 image tiles that cover a hexagonal sample area up to 200 μm wide, achieving effective pixel acquisition rates of over 1.5 GHz. Multi-beam SEM is in principle applicable to volume SEM techniques and will lead to a dramatic reduction in raw imaging time, paving the way for acquiring tissue volumes of the order of cubic millimetres and beyond.

For applications in cell or tissue biology, for which volumes of interest may be small enough to be acquired within a day or a week, the current capabilities of commercial volume SEM systems are more than enough to allow new exciting avenues of exploration. As a growing community of scientists is using these techniques, sample preparation protocols are continually being developed and improved, and software tools for data acquisition, processing and analysis are becoming more effective and user-friendly. As a consequence, the volume SEM workflow will become more robust and routine in coming years.

Volume SEM has successfully filled the 'imaging gap' that had existed in biology. Ultrastructural 3D datasets covering distances of tens or even hundreds of micrometres are becoming readily available in many laboratories. Enthusiasm about the potential of these novel techniques is justified. However, as datasets have grown in size, image processing and analysis have become the bottleneck for most studies. Relief will only come if automation fully extends into that part of the workflow.

Acknowledgements

We thank Graham Knott and Richard Schalek for valuable discussions and comments on an earlier version of the manuscript, and Stephan Gerhard, Shawn Mikula and Adrian Wanner for helpful comments on the manuscript.

Conflict of interest statement

The authors have declared no conflict of interest.

References

Ardenne, M. (1938) Das Elektronen-Rastermikroskop. Praktische Ausführung. Z. Tech. Phys. **19**, 407–416

Ballerini, M., Milani, M., Costato, M., Squadrini, F. and Turcu, I.C. (1997) Life science applications of focused ion beams (FIB). Eur. J. Histochem. **41(Suppl 2)**, 89–90

Bang, B.G. and Bang, F.B. (1957) Graphic reconstruction of the third dimension from serial electron microphotographs. J. Ultrastruct. Res. **1**, 138–146

Belevich, I., Joensuu, M., Kumar, D., Vihinen, H. and Jokitalo, E. (2016) Microscopy image browser: a platform for segmentation and analysis of multidimensional datasets. PLOS Biol. **14**, e1002340

Binding, J., Mikula, S. and Denk, W. (2013) Low-dosage maximum-a-posteriori focusing and stigmation. Microsc. Microanal. **19**, 38–55

Birch-Andersen, A. (1955) Reconstruction of the nuclear sites of Salmonella typhimurium from electron micrographs of serial sections. Microbiology **13**, 327–329

Bock, D.D., Lee, W.-C.A., Kerlin, A.M., Andermann, M.L., Hood, G., Wetzel, A.W., Yurgenson, S., Soucy, E.R., Kim, H.S. and Reid, R.C. (2011) Network anatomy and in vivo physiology of visual cortical neurons. Nature **471**, 177–182

Boergens, K.M. and Denk, W. (2013) Controlling FIB-SBEM slice thickness by monitoring the transmitted ion beam. J. Microsc. **252**, 258–262

Bohórquez, D., Haque, F., Medicetty, S. and Liddle, R.A. (2015) Correlative confocal and 3D electron microscopy of a specific sensory cell. J. Vis. Exp. **101**, e52918

Borrett, S. and Hughes, L. (2016) Reporting methods for processing and analysis of data from serial block face scanning electron microscopy. J. Microsc. **263**, 3–9

Briggman, K.L. and Bock, D.D. (2012) Volume electron microscopy for neuronal circuit reconstruction. Curr. Opin. Neurobiol. **22**, 154–161

Briggman, K.L. and Denk, W. (2006) Towards neural circuit reconstruction with volume electron microscopy techniques. Curr. Opin. Neurobiol. **16**, 562–570

Briggman, K.L., Helmstaedter, M. and Denk, W. (2011) Wiring specificity in the direction-selectivity circuit of the retina. Nature **471**, 183–188

Bushby, A.J., P'ng, K.M.Y., Young, R.D., Pinali, C., Knupp, C. and Quantock, A.J. (2011) Imaging three-dimensional tissue architectures by focused ion beam scanning electron microscopy. Nat. Protoc. **6**, 845–858

Cardona, A., Saalfeld, S., Schindelin, J., Arganda-Carreras, I., Preibisch, S., Longair, M., Tomancak, P., Hartenstein, V. and Douglas, R.J. (2012) TrakEM2 software for neural circuit reconstruction. PLoS ONE **7**, e38011

Chung, K., Wallace, J., Kim, S.-Y., Kalyanasundaram, S., Andalman, A.S., Davidson, T.J., Mirzabekov, J.J., Zalocusky, K.A., Mattis, J., Denisin, A.K., Pak, S., Bernstein, H., Ramakrishnan, C., Grosenick, L., Gradinaru, V. and Deisseroth, K. (2013) Structural and molecular interrogation of intact biological systems. Nature **497**, 332–337

Deerinck, T., Bushong, E., Lev-Ram, V., Shu, X., Tsien, R. and Ellisman, M. (2010) Enhancing serial block-face scanning electron microscopy to enable high resolution 3-D nanohistology of cells and tissues. Microsc. Microanal. **16**, 1138–1139

Denk, W., Briggman, K.L. and Helmstaedter, M. (2012) Structural neurobiology: missing link to a mechanistic understanding of neural computation. Nat. Rev. Neurosci. **13**, 351–358

Denk, W. and Horstmann, H. (2004) Serial block-face scanning electron microscopy to reconstruct three-dimensional tissue nanostructure. PLoS Biol. **2**, e329

Denk, W., Strickler, J.H. and Webb, W.W. (1990) Two-photon laser scanning fluorescence microscopy. Science **248**, 73–76

Eberle, A.L., Mikula, S., Schalek, R., Lichtman, J.W., Tate, M.L.K. and Zeidler, D. (2015) High-resolution, high-throughput imaging with a multibeam scanning electron microscope. J. Microsc. **259**, 114–120

Frank, J. (ed). (2006) *Electron Tomography: Methods for Three-Dimensional Visualization of Structures in the Cell*, 2nd ed. Springer, New York/London.

Giannuzzi, L.A. and Stevie, F.A. (eds). (2005) *Introduction to Focused Ion Beams: Instrumentation, Theory, Techniques, and Practice*. Springer, New York.

Gluenz, E., Wheeler, R.J., Hughes, L. and Vaughan, S. (2015) Scanning and three-dimensional electron microscopy methods for the study of *Trypanosoma brucei* and *Leishmania mexicana* flagella. Methods Cell Biol. **127**, 509–542

Goldstein, J., Newbury, D., Joy, D., Lyman, C., Echlin, P., Lifshin, E., Sawyer, L. and Michael, J. (2003) *Scanning Electron Microscopy and X-Ray Microanalysis*, 3rd ed. Kluwer Academic/Plenum Publishers, New York.

Guizar-Sicairos, M., Thurman, S.T. and Fienup, J.R. (2008) Efficient subpixel image registration algorithms. Optics Letters **33**, 156–158

Harris, K.M., Perry, E., Bourne, J., Feinberg, M., Ostroff, L. and Hurlburt, J. (2006) Uniform serial sectioning for transmission electron microscopy. J. Neurosci. **26**, 12101–12103

Hashimoto, T., Thompson, G.E., Zhou, X. and Withers, P.J. (2016) 3D imaging by serial block face scanning electron microscopy for materials science using ultramicrotomy. Ultramicroscopy **163**, 6–18

Hayat, M.A. (ed). (2000) *Principles and Techniques of Electron Microscopy: Biological Applications*, 4th ed. Cambridge University Press, Cambridge, UK/ New York.

Hayworth, K., Kasthuri, N., Schalek, R. and Lichtman, J. (2006) Automating the collection of ultrathin serial sections for large volume TEM reconstructions. Microsc. Microanal. **12**, 86

Hayworth, K.J., Morgan, J.L., Schalek, R., Berger, D.R., Hildebrand, D.G.C. and Lichtman, J.W. (2014) Imaging ATUM ultrathin section libraries with WaferMapper: a multi-scale approach to EM reconstruction of neural circuits. Front. Neural Circuits **8**, article 68.

Hayworth, K.J., Xu, C.S., Lu, Z., Knott, G.W., Fetter, R.D., Tapia, J.C., Lichtman, J.W. and Hess, H.F. (2015) Ultrastructurally smooth thick partitioning and volume stitching for large-scale connectomics. Nat. Methods **12**, 319–322

Helmchen, F. and Denk, W. (2005) Deep tissue two-photon microscopy. Nat. Methods **2**, 932–940

Helmstaedter, M. (2013) Cellular-resolution connectomics: challenges of dense neural circuit reconstruction. Nat. Methods **10**, 501–507

Helmstaedter, M., Briggman, K.L. and Denk, W. (2011) High-accuracy neurite reconstruction for high-throughput neuroanatomy. Nat. Neurosci. **14**, 1081–1090

Helmstaedter, M., Briggman, K.L., Turaga, S.C., Jain, V., Seung, H.S. and Denk, W. (2013) Connectomic reconstruction of the inner plexiform layer in the mouse retina. Nature **500**, 168–174

Helmstaedter, M. and Mitra, P.P. (2012) Computational methods and challenges for large-scale circuit mapping. Curr. Opin. Neurobiol. **22**, 162–169

Hennig, P. and Denk, W. (2007) Point-spread functions for backscattered imaging in the scanning electron microscope. J. Appl. Phys. **102**, 123101

Heymann, J.A.W., Hayles, M., Gestmann, I., Giannuzzi, L.A., Lich, B. and Subramaniam, S. (2006) Site-specific 3D imaging of cells and tissues with a dual beam microscope. J. Struct. Biol. **155**, 63–73

Horstmann, H., Körber, C., Sätzler, K., Aydin, D. and Kuner, T. (2012) Serial Section Scanning Electron Microscopy (S^3EM) on silicon wafers for ultra-structural volume imaging of cells and tissues. PLoS One **7**, e35172

Hua, Y., Laserstein, P. and Helmstaedter, M. (2015) Large-volume en-bloc staining for electron microscopy-based connectomics. Nat. Commun. **6**, 7923

Huang, B., Bates, M. and Zhuang, X. (2009) Super-resolution fluorescence microscopy. Annu. Rev. Biochem. **78**, 993–1016

Kanaya, K. and Okayama, S. (1972) Penetration and energy-loss theory of electrons in solid targets. J. Phys. Appl. Phys. **5**, 43–58

Kanemaru, T. and Oki, Y. (2015) Ultrathin sectioning with DUV-pulsed laser ablation: development of a laser ablation nano tome. Microsc. Oxf. Engl. **64**, 289–296

Kasthuri, N., Hayworth, K.J., Berger, D.R., Schalek, R.L., Conchello, J.A., Knowles-Barley, S., Lee, D., Vázquez-Reina, A., Kaynig, V., Jones, T.R., Roberts, M., Morgan, J.L., Tapia, J.C., Seung, H.S., Roncal, W.G., Vogelstein, J.T., Burns, R., Sussman, D.L., Priebe, C.E., Pfister, H. and Lichtman, J.W. (2015) Saturated reconstruction of a volume of neocortex. Cell **162**, 648–661

Kemen, T., Malloy, M., Thiel, B., Mikula, S., Denk, W., Dellemann, G. and Zeidler, D. (2015) Further advancing the throughput of a multi-beam SEM. Proc. SPIE **9424**, Metrology, Inspection, and Process Control for Microlithography XXIX, 94241U

Kizilyaprak, C., Longo, G., Daraspe, J. and Humbel, B.M. (2015) Investigation of resins suitable for the preparation of biological sample for 3-D electron microscopy. J. Struct. Biol. **189**, 135–146

Knoll, M. and Ruska, E. (1932) Das Elektronenmikroskop. Z. Phys. **78**, 318–339

Knott, G. and Genoud, C. (2013) Is EM dead? J. Cell Sci. **126**, 4545–4552

Knott, G., Marchman, H., Wall, D. and Lich, B. (2008) Serial section scanning electron microscopy of adult brain tissue using focused ion beam milling. J. Neurosci. **28**, 2959–2964

Knott, G., Rosset, S. and Cantoni, M. (2011) Focussed ion beam milling and scanning electron microscopy of brain tissue. J. Vis. Exp. **53**, e2588

Korogod, N., Petersen, C.C. and Knott, G.W. (2015) Ultrastructural analysis of adult mouse neocortex comparing aldehyde perfusion with cryo fixation. eLife **4**, e05793

Kremer, A., Lippens, S., Bartunkova, S., Asselbergh, B., Blanpain, C., Fendrych, M., Goossens, A., Holt, M., Janssens, S., Krols, M., Larsimont, J.-C., Mc Guire, C., Nowack, M.K., Saelens, X.,

Schertel, A., Schepens, B., Slezak, M., Timmerman, V., Theunis, C., VAN Brempt, R., Visser, Y. and Guérin, C.J. (2015) Developing 3D SEM in a broad biological context. J. Microsc. **259**, 80–96

Kubota, Y. (2015) New developments in electron microscopy for serial image acquisition of neuronal profiles. Microscopy **64**, 27–36

Lee, W.-C.A., Bonin, V., Reed, M., Graham, B.J., Hood, G., Glattfelder, K. and Reid, R.C. (2016) Anatomy and function of an excitatory network in the visual cortex. Nature **532**, 370–374

Leighton, S.B. (1981) SEM images of block faces, cut by a miniature microtome within the SEM – a technical note. Scan. Electron Microsc. **2**, 73–76

Lichtman, J.W. and Denk, W. (2011) The big and the small: challenges of imaging the brain's circuits. Science **334**, 618–623

Lich, B., Zhuge, X., Potocek, P., Boughorbel, F. and Mathisen, C. (2013) Bringing deconvolution algorithmic techniques to the electron microscope. Biophys. J. **104**, 500a

Maco, B., Cantoni, M., Holtmaat, A., Kreshuk, A., Hamprecht, F.A. and Knott, G.W. (2014) Semiautomated correlative 3D electron microscopy of in vivo imaged axons and dendrites. Nat. Protoc. **9**, 1354–1366

Maco, B., Holtmaat, A., Cantoni, M., Kreshuk, A., Straehle, C.N., Hamprecht, F.A. and Knott, G.W. (2013) Correlative in vivo 2 photon and focused ion beam scanning electron microscopy of cortical neurons (ed MA Fox). PLoS One **8**, e57405

Malick, L.E., Wilson, R.B. and Stetson, D. (1975) Modified thiocarbohydrazide procedure for scanning electron microscopy: routine use for normal, pathological, or experimental tissues. Stain Technol. **50**, 265–269

Marsh, B.J., Volkmann, N., McIntosh, J.R. and Howell, K.E. (2004) Direct continuities between cisternae at different levels of the Golgi complex in glucose-stimulated mouse islet beta cells. Proc. Natl. Acad. Sci. USA **101**, 5565–5570

Marx, V. (2012) High-throughput anatomy: Charting the brain's networks. Nature **490**, 293–298

McIntosh, R., Nicastro, D. and Mastronarde, D. (2005) New views of cells in 3D: an introduction to electron tomography. Trends Cell Biol. **15**, 43–51

Micheva, K.D. and Smith, S.J. (2007) Array tomography: a new tool for imaging the molecular architecture and ultrastructure of neural circuits. Neuron **55**, 25–36

Mikula, S., Binding, J. and Denk, W. (2012) Staining and embedding the whole mouse brain for electron microscopy. Nat. Methods **9**, 1198–1201

Mikula, S. and Denk, W. (2015) High-resolution whole-brain staining for electron microscopic circuit reconstruction. Nat. Methods **12**, 541–546

Moncrieff, D., Robinson, V.N.E. and Harris, L.B. (1978) Charge neutralisation of insulating surfaces in the SEM by gas ionisation. J. Phys. Appl. Phys. **11**, 2315–2325

Morgan, J.L., Berger, D.R., Wetzel, A.W. and Lichtman, J.W. (2016) The fuzzy logic of network connectivity in mouse visual thalamus. Cell **165**, 192–206

Narayan, K. and Subramaniam, S. (2015) Focused ion beams in biology. Nat. Methods **12**, 1021–1031

Nellist, P.D., Chisholm, M.F., Dellby, N., Krivanek, O.L., Murfitt, M.F., Szilagyi, Z.S., Lupini, A.R., Borisevich, A., Sides, W.H. and Pennycook, S.J. (2004) Direct sub-angstrom imaging of a crystal lattice. Science **305**, 1741

Nguyen, H.B., Thai, T.Q., Saitoh, S., Wu, B., Saitoh, Y., Shimo, S., Fujitani, H., Otobe, H. and Ohno, N. (2016) Conductive resins improve charging and resolution of acquired images in electron microscopic volume imaging. Sci. Rep. **6**, 23721

Pallotto, M., Watkins, P.V., Fubara, B., Singer, J.H. and Briggman, K.L. (2015) Extracellular space preservation aids the connectomic analysis of neural circuits. eLife **4**, e08206

Peddie, C.J. and Collinson, L.M. (2014) Exploring the third dimension: volume electron microscopy comes of age. Micron **61**, 9–19

Plaza, S.M., Scheffer, L.K. and Chklovskii, D.B. (2014) Toward large-scale connectome reconstructions. Curr. Opin. Neurobiol. **25**, 201–210

Reichelt, M., Joubert, L., Perrino, J., Koh, A.L., Phanwar, I. and Arvin, A.M. (2012) 3D reconstruction of VZV infected cell nuclei and PML nuclear cages by serial section array scanning electron microscopy and electron tomography (ed RD Everett). PLoS Pathog. **8**, e1002740

Robinson, V.N.E. (1975) The elimination of charging artefacts in the scanning electron microscope. J. Phys. [E] **8**, 638–640

Saalfeld, S., Cardona, A., Hartenstein, V. and Tomancak, P. (2009) CATMAID: collaborative annotation toolkit for massive amounts of image data. Bioinformatics **25**, 1984–1986

Saalfeld, S., Fetter, R., Cardona, A. and Tomancak, P. (2012) Elastic volume reconstruction from series of ultra-thin microscopy sections. Nat. Methods **9**, 717–720

Schalek, R., Kasthuri, N., Hayworth, K., Berger, D., Tapia, J., Morgan, J., Turaga, S., Fagerholm, E., Seung, H. and Lichtman, J. (2011) Development of high-throughput, high-resolution 3D reconstruction of large-volume biological tissue using automated tape collection ultramicrotomy and scanning electron microscopy. Microsc. Microanal. **17**, 966–967

Schalek, R., Wilson, A., Lichtman, J., Josh, M., Kasthuri, N., Berger, D., Seung, S., Anger, P., Hayworth, K. and Aderhold, D. (2012) ATUM-based SEM for high-speed large-volume biological reconstructions. Microsc. Microanal. **18**, 572–573

Scheffer, L.K., Karsh, B. and Vitaladevun, S. (2013) Automated alignment of imperfect EM images for neural reconstruction. arXiv **1304**.6034

Schertel, A., Snaidero, N., Han, H.-M., Ruhwedel, T., Laue, M., Grabenbauer, M. and Möbius, W. (2013) Cryo FIB-SEM: volume imaging of cellular ultrastructure in native frozen specimens. J. Struct. Biol. **184**, 355–360

Schindelin, J., Arganda-Carreras, I., Frise, E., Kaynig, V., Longair, M., Pietzsch, T., Preibisch, S., Rueden, C., Saalfeld, S., Schmid, B., Tinevez, J.-Y., White, D.J., Hartenstein, V., Eliceiri, K., Tomancak, P. and Cardona, A. (2012) Fiji: an open-source platform for biological-image analysis. Nat. Methods **9**, 676–682

Schneider-Mizell, C.M., Gerhard, S., Longair, M., Kazimiers, T., Li, F., Zwart, M.F., Champion, A., Midgley, F.M., Fetter, R.D., Saalfeld, S. and Cardona, A. (2016) Quantitative neuroanatomy for connectomics in Drosophila. eLife **5**

Seligman, A.M., Wasserkrug, H.L. and Hanker, J.S. (1966) A new staining method (OTO) for enhancing contrast of lipid-containing membranes and droplets in osmium tetroxide-fixed tissue with osmiophilic thiocarbohydrazide (TCH). J. Cell Biol. **30**, 424–432

Smith, S.J. (2007) Circuit reconstruction tools today. Curr. Opin. Neurobiol. **17**, 601–608

Sommer, C., Straehle, C., Kothe, U. and Hamprecht, F.A. (2011) Ilastik: interactive learning and segmentation toolkit. IEEE International Symposium on Biomedical Imaging: From Nano to Macro. 230–233

Soto, G.E., Young, S.J., Martone, M.E., Deerinck, T.J., Lamont, S., Carragher, B.O., Hama, K. and Ellisman, M.H. (1994) Serial section electron tomography: a method for three-dimensional reconstruction of large structures. NeuroImage **1**, 230–243

Spurr, A. (1969) A low-viscosity epoxy resin embedding medium for electron microscopy. J. Ultrastruct. Res. **26**, 31–43

Starborg, T., Kalson, N.S., Lu, Y., Mironov, A., Cootes, T.F., Holmes, D.F. and Kadler, K.E. (2013) Using transmission electron microscopy and 3View to determine collagen fibril size and three-dimensional organization. Nat. Protoc. **8**, 1433–1448

Stäubli, W. (1963) A new embedding technique for electron microscopy, combining a water-soluble epoxy resin (Durcupan) with water-insoluble Araldite. J. Cell Biol. **16**, 197–201

Studer, D. and Gnaegi, H. (2000) Minimal compression of ultrathin sections with use of an oscillating diamond knife. J. Microsc. **197**, 94–100

Tapia, J.C., Kasthuri, N., Hayworth, K.J., Schalek, R., Lichtman, J.W., Smith, S.J. and Buchanan, J. (2012) High-contrast en bloc staining of neuronal tissue for field emission scanning electron microscopy. Nat. Protoc. **7**, 193–206

Terasaki, M., Shemesh, T., Kasthuri, N., Klemm, R.W., Schalek, R., Hayworth, K.J., Hand, A.R., Yankova, M., Huber, G., Lichtman, J.W., Rapoport, T.A. and Kozlov, M.M. (2013) Stacked endoplasmic reticulum sheets are connected by helicoidal membrane motifs. Cell **154**, 285–296

Titze, B. (2013) Techniques to prevent sample surface charging and reduce beam damage effects for SBEM imaging. Dissertation. University of Heidelberg.

Titze, B. and Denk, W. (2013) Automated in-chamber specimen coating for serial block-face electron microscopy. J. Microsc. **250**, 101–110

Wacker, I. and Schroeder, R.R. (2013) Array tomography. J. Microsc. **252**, 93–99

Wanner, A.A., Genoud, C., Masudi, T., Siksou, L. and Friedrich, R.W. (2016) Dense EM-based reconstruction of the interglomerular projectome in the zebrafish olfactory bulb. Nat. Neurosci. **19**, 816–825

Wanner, A.A., Kirschmann, M.A. and Genoud, C. (2015) Challenges of microtome-based serial block-face scanning electron microscopy in neuroscience. J. Microsc. **259**, 137–142

Wei, D., Jacobs, S., Modla, S., Zhang, S., Young, C.L., Cirino, R., Caplan, J. and Czymmek, K. (2012) High-resolution three-dimensional reconstruction of a whole yeast cell using focused-ion beam scanning electron microscopy. BioTechniques **53**, 41–48

White, J.G., Southgate, E., Thomson, J.N. and Brenner, S. (1986) The structure of the nervous system of the nematode *Caenorhabditis elegans*. Philos. Trans. R Soc. Lond. A **314**, 1–340

Willingham, M.C. and Rutherford, A.V. (1984) The use of osmium-thiocarbohydrazide-osmium (OTO) and ferrocyanide-reduced osmium methods to enhance membrane contrast and preservation in cultured cells. J. Histochem. Cytochem. **32**, 455–460

Zankel, A., Wagner, J. and Poelt, P. (2014) Serial sectioning methods for 3D investigations in materials science. Micron **62**, 66–78

Received: 25 March 2016; Revised: 13 July 2016; Accepted: 14 July 2016; Accepted article online: 18 July 2016